

Excitation of a global plasma mode by an intense electron beam in a dc discharge

D. Sydorenko

University of Alberta, Edmonton, Alberta T6G 2E1, Canada

I. D. Kaganovich

Princeton Plasma Physics Laboratory, Princeton University, Princeton, New Jersey 08543, USA

P. L. G. Ventzek and L. Chen

Tokyo Electron America, Inc., Austin, Texas 78741, USA

Interaction of an intense electron beam with a finite-length, inhomogeneous plasma is investigated numerically. The plasma density profile is maximal in the middle and decays towards the plasma edges. Two regimes of the two-stream instability are observed. In one regime, the frequency of the instability is the plasma frequency at the density maximum and plasma waves are excited in the middle of the plasma. In the other regime, the frequency of the instability matches the local plasma frequency near the edges of the plasma and the intense plasma oscillations occur near plasma boundaries. The latter regime appears sporadically and only for strong electron beam currents. This instability generates copious amount of suprathermal electrons. The energy transfer to suprathermal electrons is the saturation mechanism of the instability.

PACS numbers: 52.35.Qz, 52.40.Mj, 52.65.-y

I. INTRODUCTION

Beam-plasma instabilities can produce strong electromagnetic fields which decelerate and scatter beam electrons within distances much shorter than the collisional mean free path and transfer the beam energy to plasma electrons. This process is important for wave-particle interactions, [1–4] solar disruptions, [5] inertial fusion, [6–8] collisionless shocks, [9–12] generation of suprathermal electrons, [13] *etc.* In laboratory plasmas it is often necessary to control where and how the electron beam delivers its energy to the plasma. This is especially important for advanced plasma processing applications in order to produce high-aspect ratio nano-features of electronic devices. [14, 15]

One way to control the beam energy deposition in plasma is by profiling the background plasma density. [6] Conditions favorable for development of the beam-plasma instabilities depend on parameters such as the beam and plasma densities, plasma temperature, and plasma density gradients. By appropriately controlling the choice of system parameters, it is possible to produce instabilities and beam energy deposition in desirable regions, while suppressing instabilities in undesirable regions.

Furthermore, to suppress the Langmuir waves outside the deposition region, steep plasma density gradients can be formed there to employ convective stabilization effects. [16] Several experiments indicate that electron beams can be efficiently transported through inhomogeneous plasmas for sufficiently steep plasma density gradients. In this case, the beam deposits its energy in the region of homogenous plasma density. [17]

In bounded plasmas, interaction of the beam with the plasma of uniform density can be described by the mod-

ified Pierce theory. [18, 19] This theory predicts that the amplitude of oscillations grows exponentially along the beam path. Plasma nonuniformity can completely change the development of the instability. Simulation of interaction of an electron beam with an inhomogeneous finite-length plasma discussed in the present paper reveals a different mode where intense oscillations appear only near the plasma edges, with practically no plasma wave excited in the middle of plasma. The oscillations at the opposite boundaries are synchronized. Below, this mode is referred to as the global mode.

Similar regimes have been considered before. It is known that in a finite-size plasma an eigenmode is excited due to reflection from boundaries. [20, 21] There are a number of experiments [22–25] and simulations [26, 27] where standing waves are excited by an electron beam in such a plasma. A possible mechanism of excitation of the standing wave is as follows. As beam electrons interact with the plasma wave, the wave modulates the beam velocity when the beam enters the plasma. Then bunching of the beam electrons takes place while they travel through the plasma (similar to a klystron); at the exit from the plasma the electron beam decelerates and transfers its energy to the oscillations. A wave reflects from the boundary and propagates backwards to the beam injection location. This provides the feedback between the deceleration and the modulation/injection areas. [22, 23]

The present paper describes the global mode and studies the mechanism of its saturation. It is shown that the saturation occurs because of generation of a large amount of suprathermal electrons. This finding is different from earlier assumption of Ref. 27 that the mode saturates due to the loss of synchronism between the modulated beam and the plasma oscillations at the beam exit from the plasma, where the oscillations are supposed to gain their energy from the beam.

A distinct feature of the global mode is the localization of the intense electric field in the near-wall areas where the density gradient is the strongest. Previous studies of interaction of a strong, warm electron beam with an inhomogeneous, bounded plasma showed that the trapped Langmuir waves can determine the frequencies and position of the wave field even for moderate density gradients and field strengths below the threshold for Langmuir collapse. [28–30] In those studies the beam energy was relatively low, about 40 eV, and strong acceleration of plasma electrons was not observed. The present paper demonstrates that acceleration of plasma electrons can be the main mechanism of saturation of the instability.

The paper is organized as follows. Section II describes configuration and parameters of the simulated system. Section III discusses general properties of the global mode. In Section IV, comparison of multiple rates of energy input and loss is performed. A test particle study of synchronism between the beam and the global mode is described in Section V. The concluding remarks are in Section VI.

II. SIMULATION SETUP

The study of the global mode is carried out using an electrostatic particle-in-cell code. [31] The simulated plasma is bounded between two electrodes, an anode and a cathode. A one-dimensional problem is considered, where only the direction x normal to the electrode surface is resolved. The anode at $x = 0$ has a constant positive potential $U = 800$ V. The cathode at $x = 40$ mm has a constant zero potential. The plasma consists of electrons and single-charged argon ions, there is also a uniform neutral argon gas. Collisions between electrons and neutrals are included but for the processes considered below they are not important. The cathode emits a constant flux of electrons.

The initial plasma density profile is trapezoidal – maximal in the center and decaying towards the plasma edges, which is a frequent situation in a real discharge plasma. Such a plasma state is obtained as follows. A simulation starts with a uniform plasma density $n_{e,0} = 2 \times 10^{17} \text{ m}^{-3}$, electron temperature $T_{e,0} = 2$ eV, ion temperature $T_{i,0} = 0.03$ eV, no electron and ion flows, and the electron emission from the cathode turned off. The plasma evolves for 4000 ns, then the plasma state is saved as the initial state for future simulations. The ion density and the electrostatic potential profiles in the initial state are shown by red curves in Fig. 1.

In the simulation discussed below, the cathode is emitting electrons with the flux of $\Gamma_{2,e} = 5.02 \times 10^{21} \text{ m}^{-2} \text{ s}^{-1}$, the corresponding electric current density is $J_e = 803.2 \text{ A/m}^2$. The ratio of the beam density and the plasma density in the middle of the plasma is $n_b/n_{e,0} = 0.0015$. This ratio is very small and the effect of the unmodulated beam charge on plasma oscillations excited in the system is insignificant. The simulation

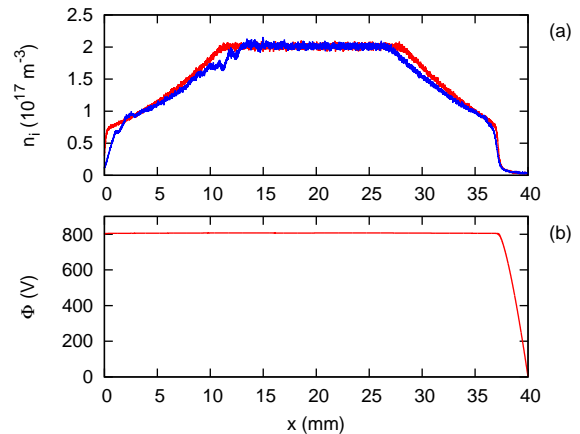


FIG. 1: (a) Profiles of ion density at $t = 49$ ns (red) and $t = 499$ ns (blue). (b) Profile of the electrostatic potential at $t = 49$ ns. Note that $t = 49$ ns is 1 ns before the emission from the cathode begins.

lasts for 500 ns, the emission starts at $t = 50$ ns.

III. GENERAL PROPERTIES OF THE GLOBAL MODE

At the very beginning of the simulation ($50 \text{ ns} < t < 100 \text{ ns}$), the two-stream instability shows an ordinary behavior, see Fig. 2(a). The beam excites oscillations with the frequency equal to the plasma frequency in the density plateau, the amplitude of the plasma oscillations grows along the direction of beam propagation, the plasma oscillations quickly decay in the plasma density gradient areas, and saturation of the instability occurs when there is strong trapping of both the beam and the bulk electrons. One can estimate the growth rate of this instability using equation (18) of Ref. 18. With $L = 17$ mm corresponding to the width of the density plateau, $\alpha \equiv n_b/n_{e,0} = 0.0015$, and the beam velocity corresponding to the 800 V accelerating voltage, one obtains the growth rate of $0.01\omega_{pe,0}$, where $\omega_{pe,0} = 2.52 \times 10^{10} \text{ s}^{-1}$ is the plasma frequency in the density plateau region. Exponential growth with this rate matches well the actual dependence of the electric field amplitude on time, compare the blue and the red curves in Fig. 3(a). Note that this growth rate is an order of magnitude lower than the classical growth rate of the two-stream instability in an infinite plasma, $0.69(n_b/n_{e,0})^{1/3}\omega_{pe,0} = 0.079\omega_{pe,0}$, compare the blue and the green curves in Fig. 3(a). The ordinary two-stream instability is similar to the one considered in Ref. 32 and is out of the scope of the present paper.

During time interval $130 \text{ ns} < t < 180 \text{ ns}$, intense oscillations occur near the plasma edges while oscillations in the middle area are much weaker. The temporal growth rate of these oscillations is about $0.0052\omega_{pe,0}$ which is lower than that of the ordinary two-stream in-

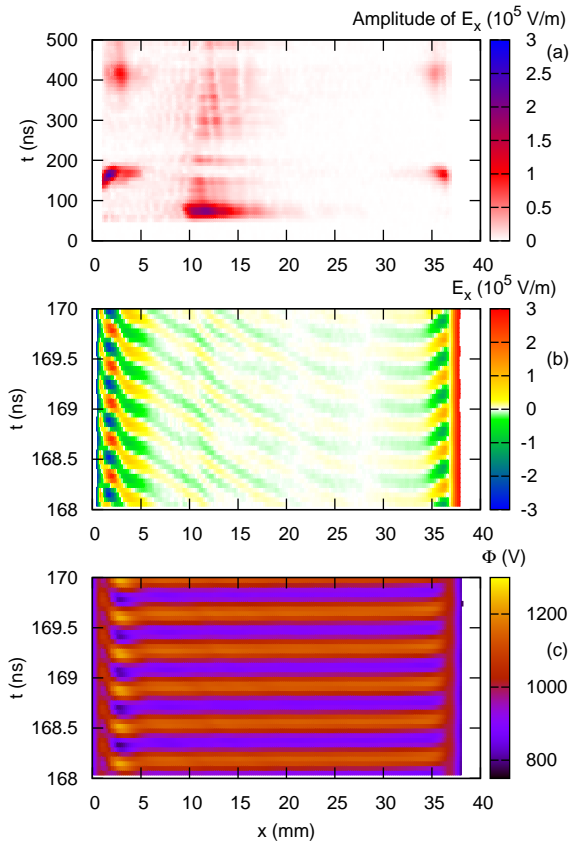


FIG. 2: (a) Electric field amplitude of high frequency plasma oscillations vs coordinate and time. Electric field (b) and electrostatic potential (c) of the global mode vs coordinate and time.

stability calculated above. This value is obtained by approximating the electric field amplitude versus time curve with an exponential law, compare the red and blue curves in Fig. 3(b). Similar regime reappears again at $390 \text{ ns} < t < 450 \text{ ns}$. This is the so-called global mode. The intermittent appearance of this mode has been observed by the authors in other simulations (not shown). An important condition for such a mode is sufficiently high current of electron emission from the cathode. Below, only the first occurrence of the global mode is considered since it is characterized by the highest amplitude.

This instability is not the ordinary two-stream instability that appears at the beginning of the simulation. Operation of the plasma beam system in the global mode resembles operation of a klystron, as suggested in Ref. 22. The velocity of the electron beam particles is modulated by plasma oscillations near the cathode. The amplitude of the velocity modulation barely grows along the beam up until it approaches the anode, see Figs. 4(a,b). Here the beam transfers its energy to plasma oscillations. These intense oscillations accelerate bulk electrons to suprathermal energies, see the enhanced high-energy tails of electron velocity distribution functions (EVDF)

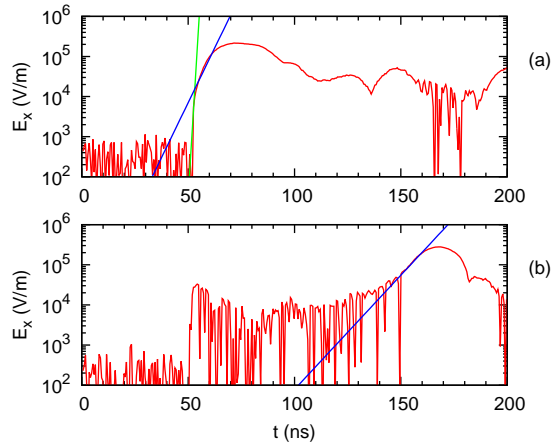


FIG. 3: Electric field amplitude of high frequency plasma oscillations vs time at points with coordinate $x = 12 \text{ mm}$ (a) and $x = 2 \text{ mm}$ (b). In (a), the green curve represents exponential growth of the two-stream instability in an infinite plasma with the rate of $0.69(n_b/n_{e,0})^{1/3}\omega_{pe,0} = 0.079\omega_{pe,0}$, the blue curve represents exponential growth with the rate of $0.01\omega_{pe,0}$. In (b), the blue curve represents exponential growth with the rate of $0.0052\omega_{pe,0}$.

shown in Fig. 4(c).

The structure of the global mode's electric field is rather complex. In most of the plasma bulk area there are short waves propagating towards the anode, they are associated with the density perturbations carried by the modulated beam. The phase velocity of these waves is equal to the average velocity of the beam. The short waves are clearly visible in the electric field, see Fig. 2(b). At the same time, Fig. 2(c) shows fast long-wavelength perturbations in the potential. They ensure the feedback between the oscillations near the anode and the cathode. These probably correspond to the uniform time dependent component of the electric field that is part of the Pierce solution [18, 19] and appear to satisfy boundary conditions.

The frequency with maximal amplitude $\omega_0 = 1.71 \times 10^{10} \text{ s}^{-1}$ is lower than the plasma frequency in the middle of the plasma $\omega_{pe,0} = 2.52 \times 10^{10} \text{ s}^{-1}$, see the spectrum in Fig. 5(a). The spectrum also reveals the presence of higher harmonics of the main frequency $2\omega_0, 3\omega_0$, etc., and the frequency of the beam resonance with the plasma in the density plateau $\omega_{pe,0}$. These frequencies have lower amplitude. The main frequency of the global mode ω_0 is detected in the spectrum everywhere along the system. The amplitude of the potential oscillations is maximal where the main frequency ω_0 is equal to the local electron plasma frequency ω_e (compare positions of the electric field spikes in Fig. 5(c) with positions of intersections between the plasma frequency profile and the main instability frequency line in Fig. 5(b)).

It is necessary to emphasize that such a regime with exactly two resonant locations $\omega_e(x) = \omega_0$ establishes if (i)

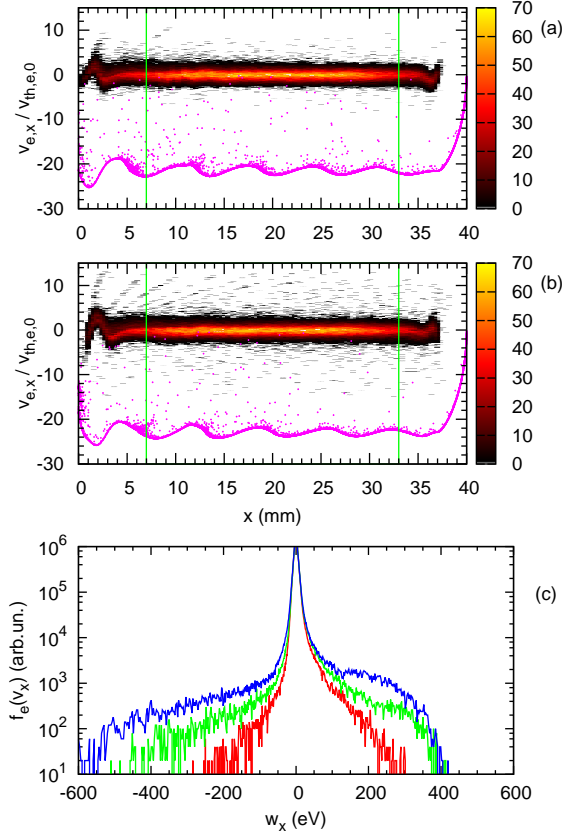


FIG. 4: (a,b) Phase planes “coordinate-velocity” of the plasma bulk electrons (colormap) and the beam electrons (magenta) at time $t_A = 160$ ns (a) and $t_C = 174$ ns (b); the scale of the velocity axis is in units of $v_{th,e,0} = (2T_{e,0}/m_e)^{1/2}$. (c) The EVDF of bulk electrons at times t_A (red), $t_B = 166$ ns (green), and t_C (blue); the horizontal coordinate axis is in energy units, the negative values of the energy correspond to propagation in the negative x -direction. Times $t_{A,B,C}$ are marked by arrows A, B, and C in Figure 6(a), respectively.

there are two areas with oppositely directed plasma gradients covering same range of plasma frequencies $\omega_{e,1} < \omega_e < \omega_{e,2}$, (ii) between these areas the plasma density has a lower limit so that $\omega_e > \omega_{e,2}$, and (iii) outside these areas the plasma density has an upper limit so that $\omega_e < \omega_{e,1}$. The electric field of the global mode shown in Fig. 2(b) has the phase of the maximal electric field near the cathode leading by about 90° relative to that near the anode. In this case, a bunch of beam electrons passes through the strongest decelerating field near the anode if

$$n(2\pi v_b/\omega_0) = L_0, \quad (1)$$

where n is a positive integer number, L_0 is the distance between points with $\omega_e = \omega_0$, v_b is the average electron beam velocity, and $2\pi v_b/\omega_0$ represents the distance between neighbor electron bunches. Understanding that L_0 is a function of the density profile and ω_0 , and that the two points defining the L_0 must be taken inside the two

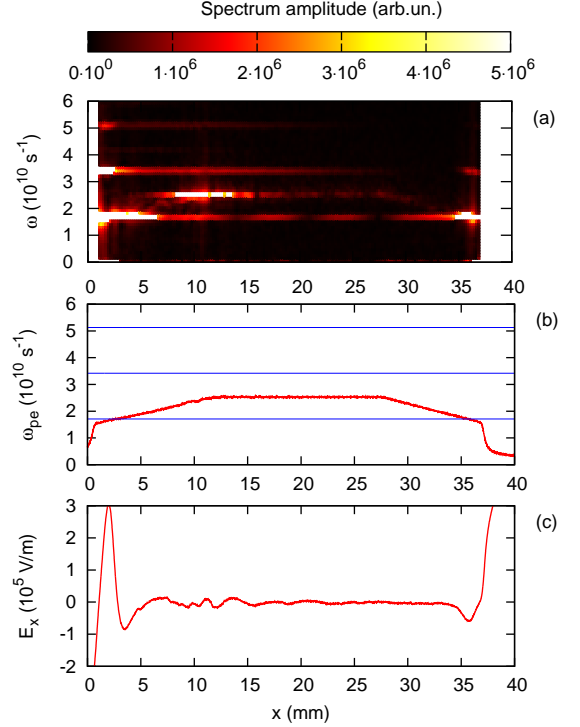


FIG. 5: (a) Frequency spectrum of plasma oscillations as a function of coordinate. (b) Profile of the electron plasma frequency $\omega_{pe} = (ne^2/m_e\epsilon_0)^{1/2}$ calculated with the ion density $n = n_i(x, t)$ (red), the three horizontal blue lines mark harmonics ω_0 , $2\omega_0$, and $3\omega_0$ of the main frequency of the instability $\omega_0 = 1.71 \times 10^{10} \text{ s}^{-1}$. (c) Profile of the electric field. The spectrum in (a) is obtained for the time interval $154 \text{ ns} < t < 178 \text{ ns}$, the profiles in (b) and (c) are at time $t = 166$ ns corresponding to the maximum of the instability.

density gradient areas specified above, one may use (1) to find possible values of the global mode frequency ω_0 . Note that there may be more than one solution satisfying $\omega_{e,1} < \omega_0 < \omega_{e,2}$ for several n , as well as no solutions at all. For the electron plasma frequency profile shown in Fig. 5(b), one can easily check that equation (1) is satisfied for $\omega_0 = 1.71 \times 10^{10} \text{ s}^{-1}$ with v_b corresponding to the bunch energy of 900 eV (plasma potential relative to cathode at $t = 160$ ns, see Fig. 6(b)), $L_b = 32.7$ mm, and $n = 5$.

Finally, it is necessary to mention that the trapezoidal profile shown in Fig. 1(a) is not the only one allowing existence of the global mode. The authors observed this mode in other simulations (not shown) where the density profile was non-trapezoidal, with more than one maximum, but still satisfied the three requirements above.

IV. ENERGY BALANCE ANALYSIS

The amplitude of electric field of the global mode both near the cathode and the anode reaches its maximum at time 167 ns, see Fig. 6(a). The growth and subsequent

decay of the global mode is accompanied by the gradual growth of the plasma potential relative to the cathode, see Fig. 6(b). This growth is caused by continuous acceleration of electrons to suprathermal energies in the near-wall areas where the electric field of the global mode is maximal, see the electron phase planes before and after saturation in Figs. 4(a) and 4(b), respectively.

The source of energy for these processes is the anode-cathode voltage U . The rate of energy deposited by the electron beam in the system, Q_b , can be calculated as

$$Q_b = U\Gamma_{2,e} - Q_{b,w} , \quad (2)$$

where $\Gamma_{2,e}$ is the electron flux emitted from the cathode, and $Q_{b,w}$ is the energy flux carried by the beam electrons across the anode boundary. The beam energy deposition rate Q_b grows as long as the field amplitude grows, compare the red curve in Fig. 6(d) with Fig. 6(a). This rate stays positive through the instability which agrees with the finding of Section V that the beam transfers energy to the global mode all the time. Also, this rate is much higher than rates of kinetic energy losses due to bulk electrons and ions escaping at the walls, see the green and the blue curves in Fig. 6(d), respectively. Thus, one can rule out enhanced wall losses as the reason of the saturation.

Both the kinetic and the electric field energies of the system grow through the instability, see the red and the blue curves in Fig. 6(c), respectively. The rates of growth of these energies are comparable to the rate of beam energy deposition, compare the red curve in Fig. 6(d) with the red and the blue curves in Fig. 6(e). It is reasonable to infer that the interplay between these three rates has the key to the saturation mechanism.

Note that after the instability saturates at $t = 167$ ns, the amplitude of the oscillatory electric field decays while the electric field energy continues to grow for another 10 ns, compare Fig. 6(a) with the blue curves in Figs. 6(c) and 6(e). To explain this difference, it is necessary to consider electric field energy calculated separately in (i) the near-anode and near-cathode sheath regions ($x < 0.6$ mm and $x > 37$ mm) and (ii) outside the sheath regions (0.6 mm $< x < 37$ mm). The former energy associated with the dc electric field in near-wall regions grows till $t = 180$ ns corresponding to the growth of the plasma potential, see the magenta curves in Figs. 6(c) and 6(e). The latter energy associated with the oscillating field of the global mode is much smaller than the former one and decays after $t = 167$ ns, similar to the instability amplitude, see the green curves in Figs. 6(c) and 6(e). Thus, the growth of the electric field energy in the whole system between 167 ns and 177 ns is associated with the growth of the sheath dc electric fields.

The kinetic energy increases mostly due to the growth of the number of suprathermal electrons. The sheath electric field energy also grows because the most energetic suprathermal electrons escape at the anode. The bulk electrons are accelerated to suprathermal energies by the intense oscillating fields of the global mode. Both the kinetic energy and the sheath field energy continue

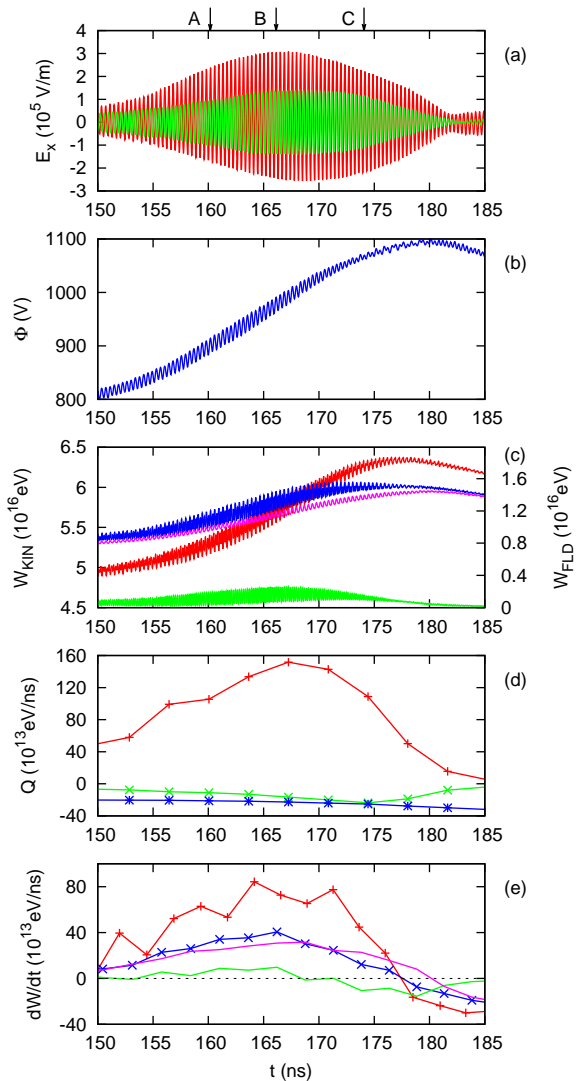


FIG. 6: Time dependencies: (a) Electric field at a point with coordinate $x = 2$ mm near the anode (red) and at a point with coordinate $x = 36.2$ mm near the cathode (green). (b) Electrostatic potential at $x = 36.8$ mm. (c) Kinetic energy (red, left vertical coordinate axis); energy of electric field in the whole system (blue), in the sheath areas (magenta, mostly dc fields), and outside the sheath areas (green, mostly plasma oscillations), all field-related curves are associated with the right vertical axis. (d) Rates of beam energy deposition in the system (red), bulk electron wall losses (green), and ion wall losses (blue); these rates are averaged over 13 oscillation periods. (e) Rates of kinetic energy variation (red), electric field energy variation in the whole system (blue), sheath electric field energy (magenta), energy of electric field of plasma oscillations (green) corresponding to the energy curves in (c) with the same color; these rates are averaged over 14 oscillation periods. In (a), arrows A, B, and C mark times when the three EVDFs shown in Fig. 4(c) are obtained.

to grow after the saturation of the instability, when the energy of the global mode decreases, compare the red (kinetic energy rate) and magenta (sheath field energy rate) curves with the green curve (global mode field energy rate) in Fig. 6(e). Therefore, it is reasonable to assume that saturation and decay of the global mode are caused by generation of suprathermal electrons.

It is interesting that while the global mode is the main channel through which the beam energy is transferred to bulk electrons, the field energy of the global mode itself is small, see the green curves in Figs. 6(c) and 6(e). This means that acceleration of suprathermal electrons is very efficient in draining the global mode energy. Indeed, the energy of suprathermal electrons reaches hundreds of eV. Most particles are accelerated in the strongest field near the anode, see Figs. 4(a) and 4(b) for $x < 5$ mm. Acceleration by the intense field near the cathode becomes noticeable after the saturation of the instability, probably because it works better for electrons with higher initial energy. Note that similar effect of enhanced acceleration of particles with higher initial energy is observed in electron acceleration by plasma waves in nonuniform plasma density. [32] One can see “threads” of electrons accelerated near the cathode in a phase plane in Fig. 4(b) for $34 \text{ mm} < x < 38 \text{ mm}$. The result of this additional acceleration is the asymmetry of the bulk EVDF with significantly higher energy of electrons flying towards the anode, see Fig. 4(c).

V. TEST PARTICLE STUDY OF BEAM SYNCHRONISM

Previously it was pointed out that changes in the regimes of standing waves excited by electron beams in plasma are associated with breaking of synchronism between modulation of the beam and the beam energy transfer to the oscillations. [27] In order to check whether the saturation of the global mode occurs because the synchronism between the modulated electron beam and the plasma oscillations near the anode is disrupted, the following numerical experiment is carried out. Test electron particles are emitted from the cathode and travel towards the anode under the influence of spatially and temporally varying electric fields extracted from the self-consistent simulation. Modulation of the velocity of test particles occurs and it results in bunching of the particles.

It is found that the bunches usually arrive into the decelerating phase of the electric field oscillations near the anode and therefore amplify the oscillations. For example, in Fig. 7 obtained before the global mode reached saturation, trajectories of most test particles cross the area of maximal oscillating field ($1 \text{ mm} < x < 2.4 \text{ mm}$) when the electric field there is negative. A similar picture is observed during the decay of the global mode, compare Fig. 8 with Fig. 7.

For further analysis, location $x = 2$ mm is selected as a point close to the center of the near-anode area with max-

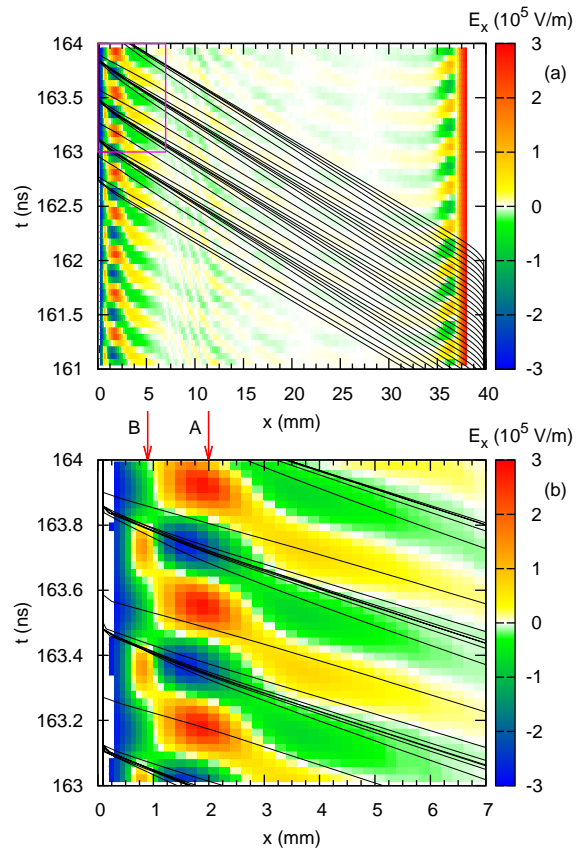


FIG. 7: (a) The color map of the electric field versus time and coordinate before the saturation of the instability. Black curves are trajectories of test particles injected from the cathode at $x = 40$ mm. Panel (b) is the magnified view of the area inside the pink box in (a). Arrow A marks location where time dependencies in Fig. 9(b) are obtained. Arrow B marks location where the beam travels through the accelerating phase of plasma oscillations.

imal oscillating field of the global mode. In the trajectory plots in Figs. 7(b) and 8(b), this location is marked with arrow A. During both the growth and the decay stages, the peak of the test particle beam density occurs very close to the negative maximum of the electric field (which is the decelerating field for electrons coming from the cathode), see Figs. 9(b) and 9(c). In fact, during virtually the whole instability interval, the product of the test particle beam current and the electric field at this location is negative, corresponding to energy transfer from the beam to the wave, see Fig. 9(a).

It is useful to mention that there is another maximum of the oscillatory field near the anode, near $x = 0.8$ mm, marked by arrow B in Figs. 7(b) and 8(b). The electric field there has opposite direction compared to the main peak marked by arrow A. As a result, the beam bunches cross this peak when the electric field is accelerating. This means that the beam takes back some energy from the field. However, the field amplitude there is lower

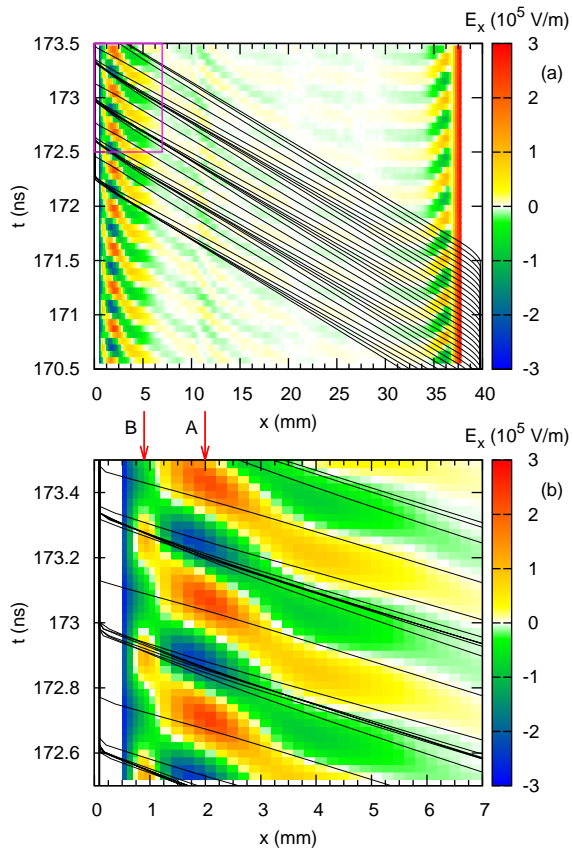


FIG. 8: Same as Fig. 7 for a different time interval, during the decay stage of the instability. Arrow A marks location where time dependencies in Fig. 9(c) are obtained.

than in the main peak and the width is smaller as well, see Figs. 7(b) and 8(b). Therefore, it is safe to assume that the effect of this small field is minor.

Thus, in contrast to what was suggested in Ref. 27, the test particle study shows that in the case considered, breaking of the synchronism between the beam and the wave is not the reason for the saturation of the global mode. The breaking of the synchronism does not occur as long as equation (1) has a solution for the given integer number n . It is the gradient of the density which allows the system to find such a solution when the velocity of electron bunches v_b increases due to the growth of the plasma potential. In simulation, the mode adjusts its frequency by gradually shifting the intense field areas closer to each other, see Fig. 2(a), which increases local values of plasma density and frequency, see Fig. 5(b). The frequency adjustment does not have to be large. For example, the beam phase planes shown in Fig. 4(a) and Fig. 4(b) both show five bunches within the gap between the intense high-frequency field areas, corresponding to $n = 5$ in (1), while there is 150 Volts difference in the plasma potential. One can easily estimate that this requires increase of the mode frequency by less than one

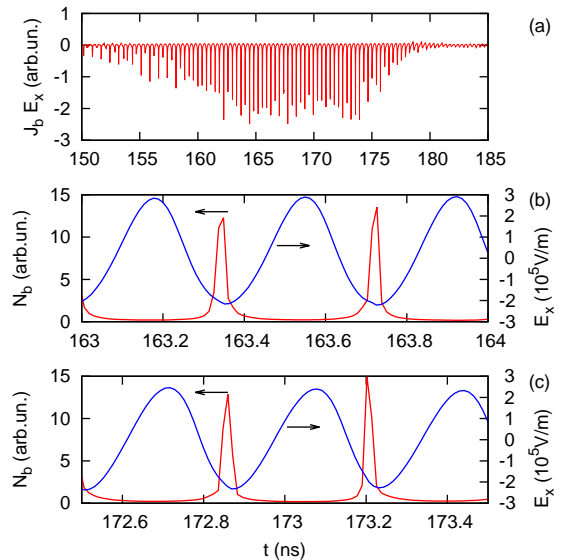


FIG. 9: (a) Losses of test particle beam energy at the point with coordinate $x = 2$ mm marked by arrow A in Figs. 7(b) and 8(b). (b) Test particle beam density (red curve, left coordinate axis) and electric field (blue curve, right coordinate axis) during time interval corresponding to Fig. 7(b). (c) Same as (b) but during time interval corresponding to Fig. 8(b).

percent.

VI. CONCLUSIONS

The global mode considered in this paper is an interesting regime when intense plasma oscillations at the opposite plasma boundaries are synchronized and the beam-plasma system operates similar to a klystron. This regime is intermittent, with on and off periods. Sometimes it co-exists with the ordinary two-stream instability, sometimes it completely replaces it. The global mode requires relatively high beam current, which is more than 800 A/m^2 in the simulation considered above. Simulations with few times lower current and otherwise similar initial state do not reveal this mode, see Ref. 32.

A detailed study of the intermittency of the global mode is beyond the scope of the present paper. One possible reason may be associated with variation of the density profile which creates or destroys favorable conditions for the instability defined by equation (1). It is necessary to mention that three major factors affecting the density profile in this study are (a) acceleration of ions towards the walls due to the ambipolar electric field which shrinks the plateau and reduces the density elsewhere, (b) escape of ions at the cathode which reduces the width of the plasma slab, and (c) ponderomotive effect of intense high-frequency electric fields which creates localized perturbations with short spatial scale. The den-

sity profile in the end of the simulation formed as a result of these factors is shown by the blue curve in Fig. 1(a).

Although the global mode appears for short periods, it is very efficient in producing suprathermal electrons, which may be critical for some applications. This paper finds that generation of the suprathermal electrons is the actual mechanism of saturation of the global mode, rather than previously suggested disruption of synchro-

nism between the beam and the wave.

ACKNOWLEDGMENTS

D. Sydorenko and I. D. Kaganovich are supported by the U.S. Department of Energy.

-
- [1] V. N. Tsytovich, *Nonlinear effects in plasma* (Plenum Press, NY, 1970).
- [2] M. Porkolab and R. P. H. Chang, *Rev. Modern Phys.* **50**, 745 (1978).
- [3] V. D. Shapiro and V. I. Shevchenko, “Basic plasma physics,” (North Holland Phys. Publ., Amsterdam, 1984) pp. 123–182.
- [4] P. A. Robinson, *Rev. Modern Phys.* **69**, 507 (1997).
- [5] D. B. Melrose, “Instabilities in space and laboratory plasmas,” (Cambridge University Press, 1986) Chap. 3, 4.
- [6] V. M. Malkin and N. J. Fisch, *Phys. Rev. Lett.* **89**, 125004 (2002).
- [7] A. J. Kemp, Y. Sentoku, V. Sotnikov, and S. Wilks, *Phys. Rev. Lett.* **97**, 235001 (2006).
- [8] A. J. Kemp, B. I. Cohen, and L. Divol, *Phys. Plasmas* **17**, 056702 (2010).
- [9] P. J. Kellogg, *Planet. Space Sci.* **51**, 681 (2003).
- [10] R. A. Treumann, *Astron. Astrophys. Rev* **17**, 409 (2009).
- [11] T. Morita, Y. Sakawa, Y. Kuramitsu, S. Dono, H. Aoki, H. Tanji, T. Kato, Y. T. Li, Y. Zhang, X. Liu, J. Y. Zhong, N. Woolsey, H. Takabe, and J. Zhang, *J. Phys. Conf. Ser.* **244**, 042010 (2010).
- [12] A. Balogh and R. A. Treumann, *Physics of Collisionless Shocks - The Space Plasma Shock Waves*, ISSI Scientific Report Series, Vol. 10 (Springer Media Verlag, Berlin-Heidelberg-New York, 2011).
- [13] P. H. Yoon, T. Rhee, and C.-M. Ryu, *Phys. Rev. Lett.* **95**, 215003 (2005).
- [14] L. Xu, L. Chen, M. Funk, A. Ranjan, M. Hummel, R. Bravenec, R. Sundararajan, D. J. Economou, and V. M. Donnelly, *Appl. Phys. Lett.* **93**, 261502 (2008).
- [15] L. Chen, Z. Chen, and M. Funk, *Plasma Sources Sci. Technol.* **22**, 065015 (2013), doi: 10.1088/0963-0252/22/6/065015.
- [16] D. D. Ryutov, *Sov. Phys. J. Exp. Theor. Phys.* **30**, 131 (1970).
- [17] Y. P. Golovanov, N. I. Elagin, L. P. Zakatov, A. S. Kingsep, and A. G. Plakhov, *Sov. J. Plasma Phys.* **3**, 349 (1977).
- [18] I. D. Kaganovich and D. Sydorenko, *Phys. Plasmas* **23**, 112116 (2016), doi: 10.1063/1.4967858.
- [19] D. Sydorenko, I. D. Kaganovich, P. L. G. Ventzek, and L. Chen, *Phys. Plasmas* **23**, 122119 (2016), doi: 10.1063/1.4972543.
- [20] R. C. Davidson and H. Qin, *Physics of Intense Charged Particle Beams in High Energy Accelerators* (Imperial College Press and World Scientific Publishing Co. Pte. Ltd., 2001).
- [21] R. C. Davidson, I. Kaganovich, H. Qin, E. A. Startsev, D. R. Welch, D. V. Rose, and H. S. Uhm, *Phys. Rev. ST Accel. Beams* **7**, 114801 (2004), doi: 10.1103/PhysRevSTAB.7.114801.
- [22] G. Wehner, *J. Appl. Phys.* **22**, 761 (1951).
- [23] D. H. Looney and S. C. Brown, *Phys. Rev.* **93**, 965 (1954).
- [24] L. Y. Kochmarev, A. I. Chmil’, and E. G. Shustin, *Plasma Phys. Rep.* **21**, 241 (1995).
- [25] N. Hayashi, M. Tanaka, S. Shinohara, and Y. Kawaj, *Phys. Plasmas* **2**, 3582 (1995).
- [26] I. J. Morey and R. W. Boswell, *Phys. Fluids B* **1**, 1502 (1989).
- [27] H. Matsumoto, H. Yokoyama, and D. Summers, *Phys. Plasmas* **3**, 177 (1996).
- [28] H. Gunell, J. P. Veoncoeur, N. Brenning, and S. Torven, *Phys. Rev. Lett.* **77**, 5059 (1996).
- [29] M. D. McFarland and A. Y. Wong, *Phys. Rev. Lett.* **80**, 5540 (1998).
- [30] M. Wendt, T. Klinger, C. Franck, and A. Piel, *Phys. Scr.* **63**, 62 (2001).
- [31] D. Sydorenko, *Particle-in-Cell Simulations of Electron Dynamics in Low Pressure Discharges with Magnetic Fields*, Ph.D. Thesis, University of Saskatchewan (2006).
- [32] D. Sydorenko, I. D. Kaganovich, L. Chen, and P. L. G. Ventzek, *Phys. Plasmas* **22**, 123510 (2015), doi: 10.1063/1.4937785.